J Biol Inorg Chem (2013) 18:429–440
DOI 10.1007/s00775-013-0987-3

ORIGINAL PAPER

Mechanistic insights into the superoxide–cytochrome *c* reaction by lysine surface scanning

Franziska Wegerich · Andrea Giachetti · Marco Allegrozzi · Fred Lisdat · Paola Turano

Received: 14 September 2012 / Accepted: 6 February 2013 / Published online: 3 March 2013

Abstract This study summarizes results which have been obtained by a mutational study of human cytochrome *c*. The protein can be used as a recognition element in analytical assays and biosensors for superoxide radicals since ferricytochrome *c* reacts with superoxide to form ferrocytochrome *c* and oxygen. Here lysine mutagenesis of the distal surface (i.e., of exposed residues around the Met80 axial ligand) of human cytochrome *c* was pursued to evaluate the effect of the surface charges on the reaction rate with the superoxide anion radical and on the redox properties of the heme protein. The latter feature is particularly relevant when the protein is immobilized on a negatively charged self-assembled monolayer on an electrode to be used as a biosensor. The observed effects of the mutations are rationalized through structural investigations based on solution NMR spectroscopy and computational analysis of the surface electrostatics. The results suggest the presence of a specific path that guides superoxide toward an efficient reaction site. Localized positive charges at the rim of the entry channel are effective in increasing the reaction rate, whereas diffused positive charges or charges far from this area are not effective or are even detrimental, resulting in a misguided approach of the anion to the protein surface.

Keywords Cytochrome *c* · Superoxide · Reaction rate · Redox potential · NMR

Abbreviations

HSQC	Heteronuclear single quantum coherence
MU	Mercaptoundecanol
MUA	Mercaptoundecanoic acid
XOD	Xanthine oxidase

Introduction

Superoxide radicals are produced by one-electron reduction of oxygen by several enzymes [1, 2]. The generation of this reactive radical is of physiological relevance in both animals and plants [3]. Several mechanisms, for example, superoxide dismutase catalyzed dismutation, have been developed to protect living systems from the action of these species, which are also involved in several cellular signaling pathways protecting the cells under stress conditions [4–6]. Much attention has been focused on the clarification of superoxide production by phagocytic NADPH oxidase since the radical is liberated by activated neutrophils as part of the defense systems [7]. Other areas of research are devoted to radical production during brain injuries, ageing, and ischemic situations in different tissues [8–10]. The generation of O_2^- by endothelial cells is relevant to their function; understanding the mechanisms underlying the regulated generation of O_2^- can help with the design of therapeutic strategies to tackle endothelial activation and

Electronic supplementary material The online version of this article (doi:10.1007/s00775-013-0987-3) contains supplementary material, which is available to authorized users.

F. Wegerich · F. Lisdat (✉)
Biosystems Technology, Wildau University of Applied Sciences, Wildau, Germany
e-mail: flisdat@th-wildau.de

A. Giachetti · M. Allegrozzi
CERM, University of Florence, Sesto Fiorentino, Florence, Italy

P. Turano (✉)
CERM & Department of Chemistry, University of Florence, Florence, Italy
e-mail: turano@cerm.unifi.it

dysfunction in conditions such as hypercholesterolemia, atherosclerosis, hypertension, diabetes, and heart failure [11]. Because of the widespread involvement of several reactive oxygen species in pathophysiological situations, the specific detection of individual species has received special attention.

Ferricytochrome *c* reacts with superoxide anion radical to form ferrocytochrome *c* and molecular oxygen [12]:

$$\text{Cytochrome } c\ (Fe^{3+}) + O_2^- \rightarrow \text{Cytochrome } c\ (Fe^{2+}) + O_2 \quad (1)$$

The redox reaction has been used for the detection of superoxide in solution for a long time [13, 14]. The reaction can be also confined to surfaces and combined with heterogeneous electron transfer from cytochrome *c* to electrodes to result in a sensor allowing spatially resolved measurements [15, 16]. This is advantageous, particularly in the medical area, since not only the presence of superoxide but also the time course of concentration changes become accessible, as it has been demonstrated for measurements in cell cultures [17, 18] and in vivo [19]. Cytochrome *c* is by far the most used recognition molecule for superoxide sensor construction since alternatively developed superoxide dismutase based systems [20, 21] often suffer from stability problems in real samples.

The rationale of this research is to design cytochrome *c* variants with increased rate of reaction with superoxide to construct cytochrome *c* based biosensors with higher sensitivity. Little is known about the mechanism of the interaction of the small charged radical and the non-uniformly charged redox protein. Earlier studies of the reaction of superoxide radical with human cytochrome *c* mutants [22] have highlighted that substitution of neutral or negatively charged amino acids with lysines at the protein surface is able to enhance the reaction efficiency only if the mutation occurs in selected locations, thus suggesting that specific intermolecular interactions are the basis of this reaction. The initial selection of the mutants was guided by earlier proposals [12] that the channel defined by the 50s helix and the facing area of the distal site might play an important role in the reaction with the superoxide anion. In particular, the characterization of a set of 11 mutants, namely, Y46K, A50K, A51K, Y74K, G77K, I81K, F82K, E61K, D62K, E66K, and E69K (Fig. 1), revealed four (E66K, E69K, Y74K, and F82K) with increased reaction rates with respect to the wild-type protein. E66K was the most interesting one for sensor construction, having a clearly higher sensitivity in comparison with the wild-type-based sensor while retaining high selectivity and showing good storage stability. Overall, the results obtained on this set of mutants showed that there is a strong dependence of the reaction rate on the position of the engineered surface positive charges, but the most effective sites do not fully confirm the initially proposed channel. The underlying reaction mechanism that allows reduction of ferricytochrome *c* and oxidation of superoxide remained elusive. In this article, we address the mechanistic aspects of the reaction, answering some key open questions. First of all, does the reaction occur through a long-range electron transfer process between the superoxide anion interacting with a positive surface residue and the ferric heme ion or does it require the anion to enter the heme cavity of cytochrome *c*? The ability of small anions such as CN^- and N_3^- to access the heme from the side of the M80 axial ligand (distal site) is well documented; at high concentration they are able to replace M80 from iron binding [23–25]. NMR relaxation data and molecular dynamics calculations have shown how this protein area is characterized by a relatively high mobility [26–31] that may facilitate the entry of the anions to the distal site. Moreover, what are the crucial protein surface properties and what makes some positions on the protein surface more effective than others in promoting this reaction?

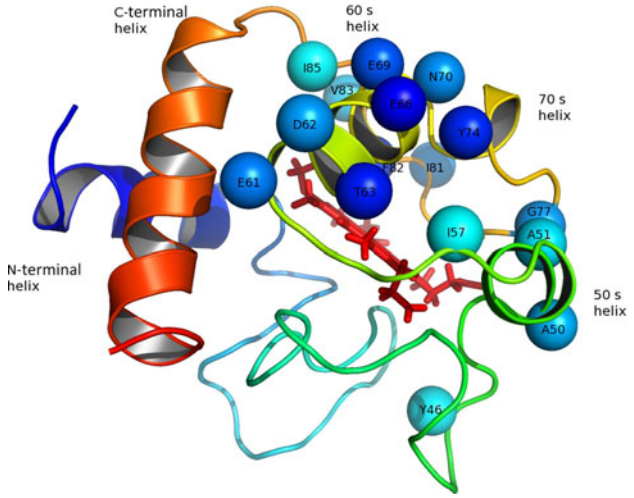

Fig. 1 Ribbon representation of the peptide part of human cytochrome *c*. The heme skeleton is shown as *red sticks*. *Blue spheres* are used to identify the residues mutated into lysine (and arginine in the case of residues 63 and 66) to scan the protein surface searching for productive guidance of superoxide anion. A color gradient is used to represent the measured differences in the reaction rate, which increases on going from *light blue* to *dark blue*

To address these issues, we prepared and characterized a new set of nine mutants. Five new single lysine mutations (I57K, T63K, N70K, V83K, I85K) were produced with the aim of scanning a larger portion of the protein surface and of defining the surface active area. Two double lysine mutations (T63K-E66K, E66K-F82K) at the most reactive positions were designed with the aim of exploiting

cooperative effects. Finally, two single arginine mutations (T63R, E66R) were characterized. Comparison of single lysine and single arginine mutants at the key sites 63 and 66 was addressed to gain insight into the electron pathway.

The new mutants were investigated in the reaction with superoxide radicals in solution and with respect to their electrochemical properties. In addition, one-dimensional ^{1}H and ^{1}H–^{15}N heteronuclear single quantum correlation (HSQC) NMR experiments were performed for structural analysis. Energy minimization and surface electrostatic potential analysis provided the rationale for the observed behavior that suggests the presence of a specific path that, through localized positive charges, guides superoxide anion from an entry point on the protein surface into the distal cavity.

Materials and methods

Protein samples

Full-length human cytochrome *c* and its mutants were expressed in *Escherichia coli* and purified in the unlabeled and ^{15}N-labeled forms, as reported in the literature [22, 32].

Determination of rate constants

To guarantee ultrapure samples for the determination of the reaction rate of cytochrome *c* with superoxide, mutant and wild-type cytochrome *c* were dialyzed before the spectrophotometric kinetic measurements with 50 mM sodium phosphate buffer pH 7.5 using Slide-A-Lyzer dialyses cassettes (Thermo Scientific, Rockford, USA) with a molecular mass cutoff of 3,500 kDa. The amount of oxidized cytochrome *c* used for this measurement was calculated from the absorption spectrum of the dialyzed protein before each measurement and the total amount of cytochrome *c* in the sample which could be retrieved from the absorption spectrum of reduced cytochrome *c* (treated with dithiothreitol or sodium dithionite) (with $\varepsilon_{550\text{-ox}} = 7.4\ \text{mM}^{-1}\ \text{cm}^{-1}$ and $\varepsilon_{550\text{-red}} = 32.02\ \text{mM}^{-1}\ \text{cm}^{-1}$ determined with horse heart cytochrome *c* in 50 mM sodium phosphate buffer pH 7.5).

A steady-state superoxide concentration was generated in vitro using the enzyme xanthine oxidase (XOD) and its substrate hypoxanthine [33]. The increase of absorbance at 550 nm after addition of XOD, with a final concentration of 30 mU ml^{-1}, was recorded for 60 s in the presence of 100 μM hypoxanthine with a spectrophotometer or a stopped-flow spectrometer (SX.18MV stopped-flow reaction analyzer, Applied Photophysics, UK). This corresponds to a steady-state superoxide concentration of about 520 nM calculated using the following formula [33]:

$$[O_2^-] = \sqrt{\frac{k_g}{2k_D}[\text{XOD}]} \quad (2)$$

The rate constant for the enzymatic superoxide generation with XOD, k_g, was determined photometrically to be 0.015 μM ml s^{-1} mU^{-1}. The rate constant of spontaneous dismutation k_D ($2O_2^- + 2H^+ \rightarrow O_2 + H_2O_2$) at pH 7.5 is $2.3 \times 10^5\ M^{-1}\ s^{-1}$ [34]. The initial rate of reduction of cytochrome *c* was measured for seven different cytochrome *c* concentrations (0.2–5 μM cytochrome *c*) for each cytochrome *c* form. This was done at least twice. From the resulting plot the reaction rate constant k_1 for the reaction of cytochrome *c* and superoxide (Eq. 1) was derived.

Electrochemical measurements

Cyclic voltammetry was employed to determine thermodynamic and diffusional properties of the purified mutants. An Autolab PGSTAT 20 and a μAutolab type II potentiostat (Metrohm, Germany) were used. Electrochemical investigations with cytochrome *c* in solution were performed with mercaptopropanol-modified gold electrodes. Gold wire electrodes were cleaned following an established protocol [33]. Incubation with 20 mM mercaptopropanol was conducted for 24 h. Cyclic voltammograms were recorded with 20 μM cytochrome *c* in 1 M KCl and 10 mM sodium phosphate buffer, pH 7.0. The redox potential, E_0, was calculated as the mean of the midpoint potentials, E_f, between the anodic and cathodic peak potentials at different scan rates (50–400 mV s^{-1}). This is appropriate since E_f is almost independent of the scan rate in the range from 50 to 400 mV s^{-1}. Diffusion coefficients were calculated from the peak currents at different scan rates according to the Randles–Sevcik equation [35].

Electrochemical investigations of adsorbed cytochrome mutants on gold electrodes were also performed. Here the needle electrodes were modified with mercaptoundecanoic acid (MUA) and mercaptoundecanol (MU; incubation for 48–72 h in 5 mM solutions with a volume ratio of 1:3). Subsequently the electrodes were incubated for 2 h in 30 μM cytochrome *c* (in 5 mM potassium phosphate buffer pH 7). The heterogeneous electron transfer rate constant, k_s, was determined by cyclic voltammetry and variation of the scan rate between 100 mV s^{-1} and 15 V s^{-1}, followed by evaluation of the peak separation according to the method of Laviron [36]. The amount of redox-active cytochrome *c* (surface coverage Γ) was derived from the charge using Faraday's law. The analysis of the voltammetric curves was performed with the Autolab software (GPES versions 4.8 and 4.9).

NMR spectra

The reduced and oxidized states of the proteins were obtained by addition of dithiothreitol and excess of ferricyanide, respectively. The oxidizing agent was then removed by ultrafiltration before NMR data acquisition. The protein concentration was 200 μM for all samples, in 20 mM phosphate buffer, pH 6.8 with 10 % D_2O.

NMR experiments were conducted at 300 K using a Bruker 800 MHz spectrometer equipped with a TXI cryoprobe. One-dimensional ^1H NMR spectra for the detection of the diamagnetic part were recorded over a spectral width of 20 ppm and with a 1.2 s recycle delay, with excitation sculpting (zgesgp; Bruker library) for efficient water suppression. Detection of the hyperfine-shifted signals in the ferric form of the proteins was achieved using a larger spectral width (100 ppm), faster repetition rates (600 ms), and presaturation for water suppression. Two-dimensional ^1H–^{15}N HSQC experiments were performed with 1,024 × 256 data points, over a spectral width of 14 ppm for ^1H and 40 ppm for ^{15}N. Spectra were processed and analyzed with the Bruker TopSpin software package.

Energy minimization

The first conformer of the published family of NMR structures of reduced human cytochrome *c* [37] was used as the starting configuration for energy minimization of the variants T63K, T63R, E66K, and E66R and for the double mutant T63K-E66K. The structures of the mutant proteins were energy-minimized using AMBER [38] The AMBER ff99SB force field [39] was employed and the parameters describing the iron(II) heme were derived from previous studies [40].

The energy minimization was performed using the AMBER 10.0 implicit solvent approximation based on a generalized Born formalism [41]. The backbone conformation of all residues was fixed except for the mutated one; this choice was justified by the invariant fingerprint of the ^1H–^{15}N HSQC spectra (see later and the electronic supplementary material for further details). Two calculation steps were performed. In the first step only the side chain of the mutated residue was free to move during energy minimization, in the second step the side chains of the mutated residue and of amino acids 51–74 were allowed to change their orientations during energy minimization. Calculations were performed via the AMPS-NMR web portal [42].

Electrostatic potentials

The structures resulting from energy minimization were analyzed using the APBS tool [43] of PyMOL to derive information about the surface electrostatic potentials. The PQR input file was generated with the AMBER ambpdb utility using topology and coordinates files from the energy minimization calculation. The grid dimension for APBS was derived using the PyMOL psize.py utility, resulting in a grid of 97 × 97 × 97 points with fine mesh lengths of 61.5 Å × 59.6 Å × 56.4 Å; the default APBS tool setting was used for the calculation. The images with the electrostatic field gradient were generated with the program VMD [44] using the previous APBS-calculated electrostatic grid potential file as input. The visualization parameters were as follows: Gradientmag 8.3, min length 1.00, max length 200.00, and color scale range from −0.5 to 0.5.

Results and discussion

Reaction rate with superoxide in solution

The reaction rate constants with superoxide were determined in solution by recording the changes in absorption at 550 nm (increase in reduced cytochrome *c*) as a function of time and protein concentration. The results obtained are summarized in Table 1, where data from our previous study [22] are also reported for comparative purposes.

Among single lysine mutants, those at E61, D62, N70, G77, and I81 have reaction rates that are comparable with those of the wild-type protein; six mutants (Y46K, A50K, A51K, I57K, V83K, and I85K) show a reduced reaction rate with superoxide, whereas T63K, E66K, Y74K, and F82K show a higher rate constant in the reaction with the radical compared with the human wild-type; the E69K variant has a reaction rate constant just slightly greater than the wild-type protein. This information is mapped on the protein structure in Fig. 1. A further enhancement by combining the two "highest-rate" mutation sites is not achieved: in contrast, the double mutant T63K-E66K exhibits a decreased reaction rate with superoxide. Single arginine mutants at the highest-rate sites, namely, T63R and E66R, both have reaction rates comparable to that of the wild-type protein and therefore lower than those observed for the single lysine mutations at the same positions.

The above results clearly indicate that only specific positions are effective in augmenting the reaction rate with superoxide, whereas others are not effective or are even detrimental. As it will be detailed in the following sections, with the exception of the previously characterized Y46K, F82K, and E66K-F82K, all the mutants maintain the same spectroscopic and structural properties (as found by intact electronic absorption and NMR spectra) of the wild-type protein and only I57K and Y46K and, to a lesser extent, F82K show different redox properties. As a whole, these

Table 1 Reaction rate constant with superoxide (k_1), redox potential (E_0) in solution (derived from the scan rate dependence of the formal potential calculated as the midpoint potential from oxidation and reduction peak potentials), and diffusion coefficient (D) for horse heart cytochrome c, human wild-type cytochrome c, and its mutants

	Reaction rate with O_2^- in solution	Electrochemical properties in solution	
	$k_1/10^4$ (M^{-1} s^{-1})	E_0 (mV)	$D \times 10^6$ (cm^2 s^{-1})
Unmutated cytochrome *c*			
Horse heart	6.7	15	2.3
Human	6.6	17	1.7
Single lysine mutants			
Y46K	2.5	−40	0.9
A50K	5	13	1.3
A51K	3	14	1.9
I57K	2	−30	1.8
E61K	7	18	3.1
D62K	6	13	1.4
T63K	11.3	7	1.9
E66K	12.5	20	1.6
E69K	8.8	11	1.6
N70K	6.4	22	1.3
Y74K	10.7	15	2.6
G77K	6	12	1.5
I81K	6.5	18	1.2
F82K	10.7	2	0.4
V83K	4.3	17	1.4
I85K	2.1	18	1.9
Double lysine mutants			
E66K-F82K	2	10	0.1
T63K-E66K	1.8	10	0.3
Single arginine mutants			
T63R	6.4	15	3.2
E66R	5.3	24	1.5

Average errors on k_1, E_0, and D are $\pm$ 2 $\times$ 10^4 M^{-1} s^{-1}, $\pm$ 5 mV, and $\pm$ 0.4 $\times$ 10^6 cm^2 s^{-1}, respectively

data suggest that the introduction of an additional positive charge at certain positions results in misguiding of superoxide. In contrast, the same additional charge at other positions enhances the "productive" guidance of the radical.

Electrochemical characterization in solution

Cyclic voltammetry was performed at different scan rates to deduce the formal redox potential and the diffusion coefficients of the different mutants (Table 1). Although for most of the mutants no remarkable influence of the mutation on E_0 was observed, for I57K a value of -30 ± 5 mV versus Ag/AgCl was determined, and this is clearly below the range of the other proteins. The only other variant showing a negative E_0 is the previously characterized Y46K (-40 ± 5 mV). Therefore, one can conclude that the oxidized state of Y46K and I57K is stabilized relative to the reduced state by the mutation; this on the other hand diminishes the driving force for the superoxide oxidation and may contribute to the low reaction rate constant mentioned in the previous section. Nevertheless, a slightly diminished E_0 can be also noticed for F82K (2 ± 5 mV), for which a higher radical reaction rate has been observed [22].

The diffusion coefficients of all the mutants calculated from the voltammetric measurements are rather similar to the diffusion coefficient of the wild type and are of the same order as those already reported for the first set of mutants [22]. Only for F82K and the double mutants the values are slightly smaller.

Mutants adsorbed on gold electrodes

The thermodynamic and kinetic properties of a subset of mutants were characterized electrochemically with the proteins adsorbed on a thiol-modified gold electrode. This arrangement reflects the situation of the protein in a biosensor application in which superoxide-induced reduction of cytochrome c is coupled with a direct electron transfer between the protein and an electrode, resulting in an oxidation current proportional to the superoxide concentration.

The selected variants are the two single lysine mutants T63K and N70K, the two single arginine mutants T63R and E66R, and the double mutants T63K-E66K and E66K-F82K. In Table 2 their properties are compared with those of previously characterized variants and wild-type horse heart and human proteins. All chosen mutants can be adsorbed on the negatively charged MUA/MU layer. Figure 2 shows as an example the cyclic voltammogram of the mutant N70K, which is similar to the voltammogram obtained with the wild type.

The formal potential E_f can be calculated as the mean of the midpoint potentials between the anodic and cathodic peak potentials at low scan rates. The formal potential of adsorbed proteins lies, in general, below the formal redox potentials of the solution-state cytochrome *c*. This can be explained by the electrostatic stabilization of the more positive oxidized state over the reduced state of immobilized cytochrome *c* owing to the negatively charged self-assembled monolayer surface, which was also observed in other work [45]. Within the subset of the mutants adsorbed on MUA/MU gold electrodes, N70K and the double mutant T63K-E66K reveal the largest increase in E_f compared with the wild type. In the case of the double mutant T63K-E66K, this can be attributed to a less effective electrostatic stabilization of the oxidized state owing to a different orientation of the protein. The orientation of adsorbed cytochrome *c* on negatively charged self-assembled monolayers, proposed by Xu et al. [45, 46], is depicted in Fig. 3. Both exchanged amino acids of the double mutant—E66 and T63—are normally not visible for the electrode. In the case of the introduced positively charged lysines, it is reasonable that the two charges cause a

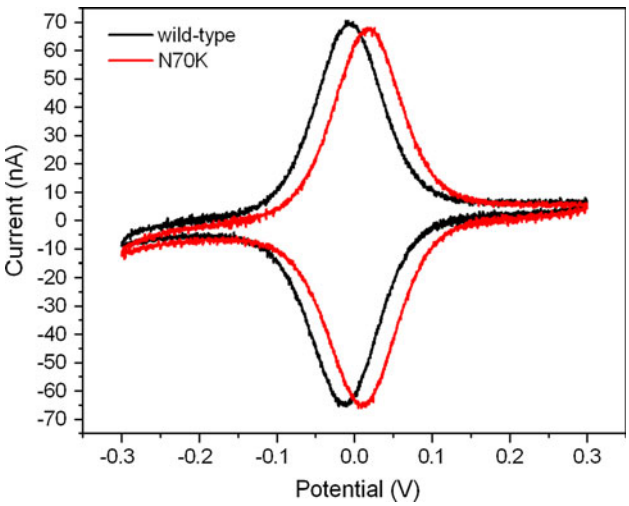

Fig. 2 Cyclic voltammograms of the mutant N70K and human wild-type cytochrome *c* adsorbed on MUA/MU-modified gold electrodes (5 mM sodium phosphate, pH 7, scan rate 100 mV s^{-1})

Table 2 Electrochemical properties of cytochrome *c* adsorbed on mercaptoundecanoic acid/mercaptoundecanol (MUA/MU) modified gold electrodes

	Electrochemical properties of cytochrome *c* adsorbed on modified Au electrodes			
	E_f (mV)	Γ (pmol cm^{-2})	k_s (s^{-1})	$E_{w1/2}$ (mV)
Unmutated cytochrome *c*				
Horse heart	−7	13	55	102
Human wild type	−8.6	10.7	61	101
Single lysine mutants				
T63K	−9.5	9.1	47	97
E66K	1	12	55	109
E69K	2	11	47	106
N70K	9.1	10.3	45	101
Y74K	0	7	113	97
F82K	−19	6	139	96
Double lysine mutants				
E66K-F82K	3.6	3.8	125	91
T63K-E66K	7.5	2.8	27	141
Single arginine mutants				
T63R	−14.8	5.6	68	110
E66R	−1.4	6.9	60	125

Values were obtained in 5 mM potassium phosphate buffer, pH 7. Average errors on E_f, Γ, k_s, and $E_{w1/2}$ are ± 5 mV, ± 3 pmol cm^{-2}, ± 8 s^{-1}, and ± 5 mV respectively

E_f is the formal potential of the surface-fixed redox protein calculated from the mean of the midpoint potentials from oxidation and reduction peak potentials detected at small scan rates, Γ is the surface concentration of electroactive cytochrome *c*, k_s is the heterogeneous electron transfer rate constant of cytochrome *c*, and $E_{w1/2}$ is half peak width of the voltammetric peaks

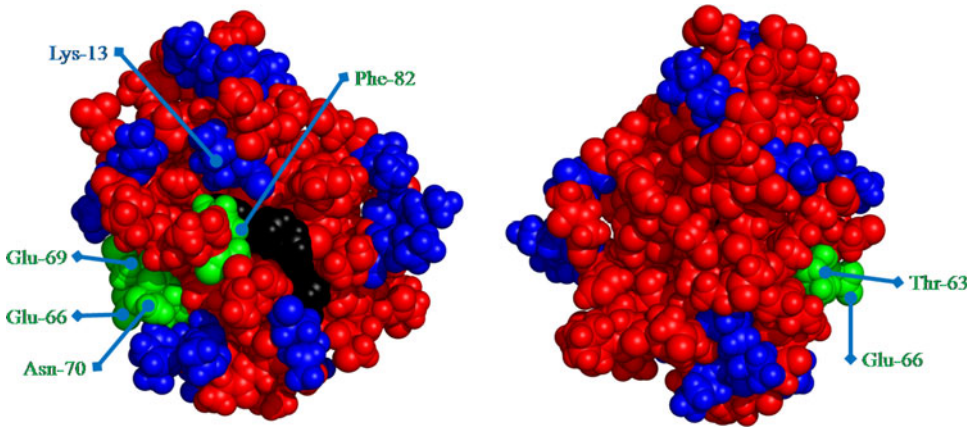

Fig. 3 Orientation of cytochrome *c* immobilized on a self-assembled monolayer modified electrode. Heme is depicted as *black spheres*, and mutation sites are depicted as *green spheres*. *Blue spheres* represent native positively charged lysine residues. *Left* view from the electrode. *Right* view from the solution. (From [30])

different orientation. This hypothesis is also supported by the decreased electron transfer rate, k_s, and the increased half peak width, $E_{w1/2}$, determined for this mutant. The different orientation can cause a less effective heterogeneous electron transfer, probably due to a larger distance between the heme and the electrode. Also the smaller amount of protein which can be adsorbed on the electrode for these mutants supports the altered situation described.

For N70K the increased formal potential without any other significantly changed feature might be due to local structural changes in the heme environment, which occur only after immobilization of the protein. A smaller amount of redox-active protein can be immobilized on the electrodes for the two arginine mutants too. Here probably the binding efficiency of the second binding region containing residues 73, 79, 87, and 88 [45, 46] is diminished owing to a charge distribution different from that of the lysine mutants near this region (vide infra). In support of the role of this second binding region, also Y74K shows a similarly reduced amount of adsorbed redox-active protein.

The mutant F82K exhibits a decreased redox potential and interestingly a drastically increased heterogeneous electron transfer rate constant. This behavior indicates a different situation on the surface originating from structural changes of the mutant compared with the wild type and is confirmed by ^{1}H NMR and ^{1}H–^{15}N HSQC data that indicate an opening of the mutant structure [22]. In addition, a different mechanism for the interaction with superoxide radicals cannot be ruled out. An analogous situation seems to hold for the double mutant T63K-F82K. Both proteins show a diminished amount of electroactive adsorbed protein on the electrode surface.

In summary, for the application of the mutants in a cytochrome *c* based radical biosensor, not only a high reaction rate with superoxide is important, but so are structural integrity allowing full surface coverage in the electrode immobilization process, unaltered redox properties, and fast electron transfer kinetics [33]. This requirement can be achieved in particular by the following mutants: T63K, T66K, T69K, and Y74K.

NMR spectra

As in our previous studies, NMR spectroscopy was used to rationalize some of the electrochemical data in terms of structural properties [22, 47] and in particular to verify the structural integrity of the cytochrome *c* mutants produced. One-dimensional ^{1}H NMR spectra and ^{1}H–^{15}N HSQC spectra of the ferrous and ferric forms of the wild-type cytochrome *c* were used as a fingerprint of the iron axial ligation and overall protein fold. For the initial set of 11 mutants [22] one-dimensional NMR spectroscopy revealed that the M80 axial ligation is maintained for all the protein variants, with the only exception being the oxidized form of F82K, where M80 is replaced with another, unidentified protein ligand. This structural transition and the subsequent changes in the electronic structure of the paramagnetic iron center induce important changes in the HSQC spectra of ferric F82K. Redox-dependent conformational changes of the same type are observed here for the double mutant, E66K-F82K (Figs. S1, S2). Important structural changes, with an essentially intact coordination, were found for both oxidized and reduced Y46K. All the other mutants exhibit only minor structural differences with respect to the wild-type cytochrome *c*.

The ^{1}H spectra of the reduced and oxidized forms of wild-type cytochrome *c* and its T63K and T63R variants point to a substantially intact axial coordination for the heme iron in both oxidation states: signals of the axial M80 ligand resonate slightly upfield in the reduced form (Fig. S1), whereas they are at around −30 ppm in the oxidized protein (not shown). For the ferric case, the shift pattern of the heme methyl signals is determined by the arrangement and nature of the axial ligands. In these mutants, the shift of the heme methyls resolved outside the diamagnetic envelope is clearly the same as for the

wild-type protein (Fig. S3), providing further proof for an intact coordination environment even in the ferric form of the protein.

The $^{1}H–^{15}N$ HSQC spectra of the reduced proteins are a fingerprint of the protein fold and show that chemical shift differences between the wild type and the mutants are small and clustered around the mutation site (Fig. S4). In particular, affected residues are located on the so-called 60s helix, which contains the mutated residue, and the two facing helices (70s and 50s); chemical shift changes are also observed for the backbone amides of residues facing the 50s helix and for the backbone and side chain NH groups of W59. Small shift variations on the same residues are observed in the HSQC spectra of the oxidized form of T63K and T63R (Fig. S5). The differences between T63K and T63R are confined to residues 52, 56, 57, 59, 66, 67, 69, and 74, and are even smaller than those between the wild type and each single mutant.

A similar situation has been reported for E66K, with NMR spectra essentially superimposable with those of the wild-type protein in both oxidation states [22]. This is also the case of E66R (Figs. S1, S3-S5).

Replacement of both T63 and E66 with lysine residues again induces very minor changes in the chemical shifts of heme substituents and axial ligands with respect to the wild-type case (Figs. S1, S3) and causes the variations in the chemical shift of backbone amides of the same regions already discussed for the single mutants (Figs. S4, S5). In summary, NMR spectroscopy proves that the overall protein fold, the axial coordination of the heme iron, and consequently the electronic structure typical of the wild-type protein are maintained in the three variants T63K, T63R, and T63K-E66R. Therefore, the observed different reactivity toward superoxide can only derive from localized changes that we simulated with the aid of energy minimization calculations.

Energy minimization and surface electrostatic potentials and fields

Human cytochrome *c* is largely positive, having a sequence that contains 18 lysine and two arginine residues but only two aspartate and eight glutamate residues. This small protein has a "face", roughly identified by the N-terminal helix, the following long loop, and the loop containing the M80 iron axial ligand, where the charged residues are only positive, whereas the other "face" shows some areas with surface-exposed negatively charged amino acid side chains, which include the 60s helix, where we introduced positive charges that were effective in facilitating the reaction with superoxide. Graphical visualization of the calculated electrostatic potentials (Figs. 4, 5) suggests a role for the artificially introduced local positive charges on the 60s helix that may provide a guide toward the heme for the superoxide anion through a sort of channel whose entrance is defined by the three α-helices (50s, 60s, and 70s) and the loop containing W59 (see also Fig. 1).

The side chain of T63 in the structure of the wild-type protein points toward the backbone NH of G60. After energy minimization calculations for the mutant proteins, the side chains of lysine in T63K and arginine in T63R assume a different orientation with respect to the side chain of the native T63. They are stabilized in the new conformation through the interaction with the side chains of D62 (Fig. 4, left). Comparison of the electrostatic surfaces around the mutation site for the energy-minimized structures of the variants T63K and T63R with that of the wild-type protein shows that in the case of the wild type, the presence of a threonine at position 63 corresponds to a large patch of negative charges, whose extension is reduced on introduction of arginine or lysine single-point mutations at this site. T63R, however, is characterized by a more distributed charge with respect to T63K. In the case of the variant E66K (and E66R) (Fig. 4, right), the side chains of lysine and arginine introduced at position 66 protrude from the surface into the bulk solvent and their positive ends reduce the negative patch typical of the wild type in this protein area. Again, substitution of E66 with an arginine gives rise to a less localized positive charge than in the case of E66K. The distributed charge observed for the arginine variants corresponds to reaction rates that are very similar to those of the wild-type protein, suggesting that a localized positive charge is needed to exert a measurable attraction for superoxide ions. Since all the experiments were performed in electrolyte solutions with a part of the charge shielded by counter ions, the small differences between the lysine and arginine mutants seem to be significant for the attraction of the radical.

In the double mutant T63K-E66K (Fig. 5), the two lysine side chains point toward D62 and the bulk solvent, respectively, thus generating a very large positive area that only marginally includes positions 66 and 63.

Surface electrostatic potentials and fields are visualized in Fig. 6. In the wild-type protein negative (red) field lines extend in an area that, at least partially, includes our proposed entry point. Introduction of a single lysine residue at position 63, and even more so at position 66, is effective in reducing the negative field lines: the proposed entry point is now characterized by the presence of positive field lines surrounded by negative ones, thus creating a sort of electrostatic tunnel that may guide the anion toward the proper position. This effect is lost in the double lysine mutant. Here a large part of the protein surface becomes positive and thus guiding of the radical anion toward the heme center cannot occur. Instead a misguiding of superoxide to other parts of the protein may occur, resulting in a decreased reaction rate constant.

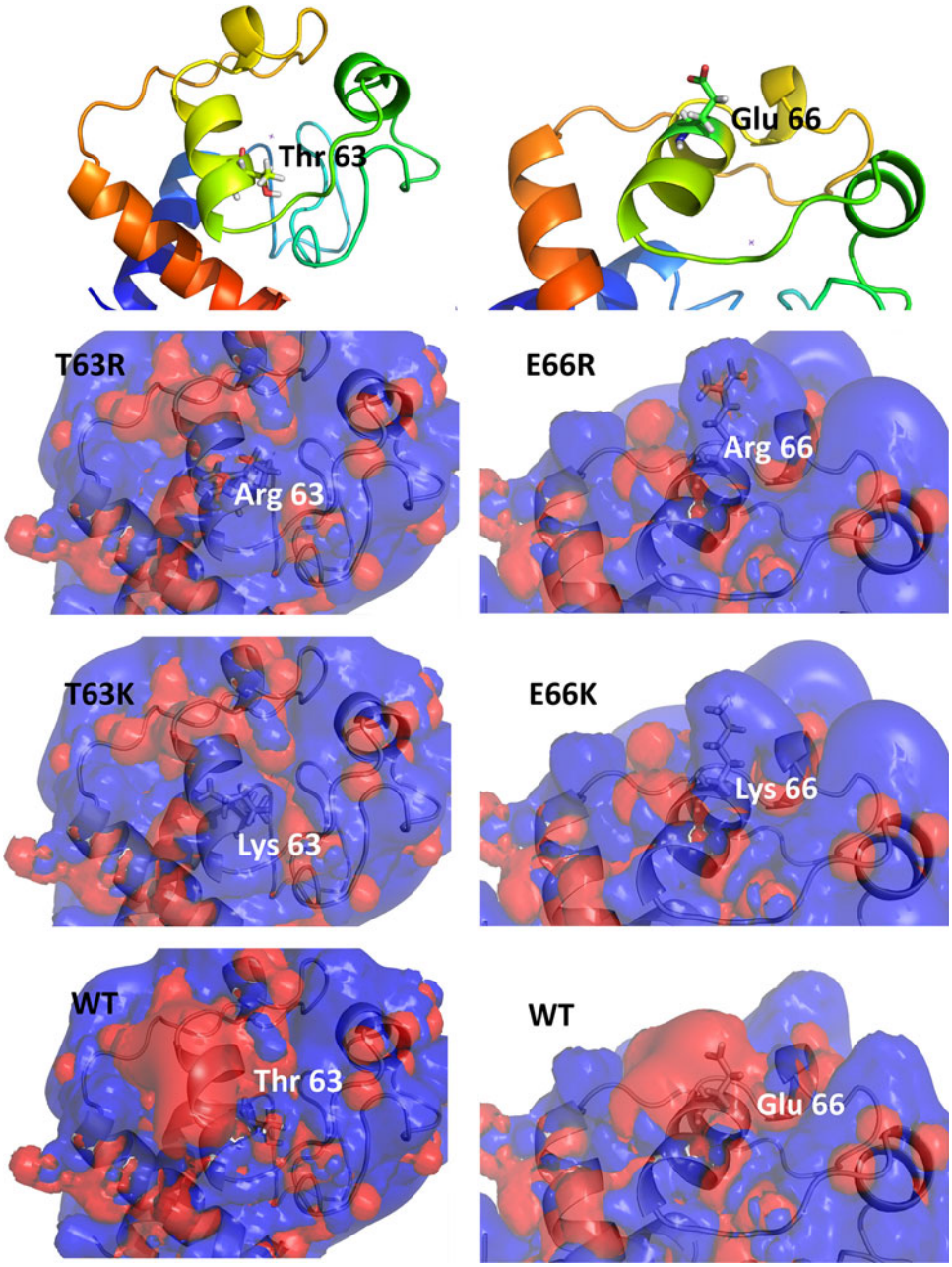

Fig. 4 Surface potential representation of the area around residue 63 (*left*) and residue 66 (*right*) in human cytochrome *c*: regions where the electrostatic potential is less than −1 *kT*/*e* are in *red*, whereas those where it is greater than 2 *kT*/*e* are in *blue* (*k* is the Boltzmann constant, *T* is absolute temperature). The structures in the *left panels* and the *right panels* have different orientations to better show the protein surface area involved. In the *top panels* the same cartoon representation as in Fig. 1 is used to help localize the analyzed areas on the whole protein structure. The mutated residues are always shown as sticks, visible in transparency in the case of surface potentials, where the residue label has been added at the terminal part of the side chain. The protein backbone, displayed using cartoons, is also shown in transparency. *WT* wild type

Conclusions

We have designed, produced, and experimentally tested a number of mutants of human cytochrome *c* which are significantly more active than the wild-type protein toward the oxidation of superoxide anion owing to improved electrostatic guidance of superoxide anion toward the heme, while maintaining unaltered overall fold and heme iron axial ligation. Upregulated mutations include those at T63, E66, and Y74, which define an entry point between the 60s and 50s helices, as shown in Fig. 7. Introduction of lysine residues at the rim of this channel increases the reaction rate with superoxide via electrostatic guidance. Positive charges far from this site are not effective, or are even detrimental, by misguiding the superoxide anion and by attracting it to sites far from its entry point. Localized charges are more effective than diffused ones. Lysines, which have a less distributed positive charge than arginines, are more effective in controlling the process. An extended positively charged surface area is created by the double lysine mutant T63K-E66K. As a consequence, this is also less efficient than the wild type since the guidance properties are lost.

Therefore, the reaction rate is not dominated by a generic long-range electrostatic attraction of the anions toward the protein surface, but by a specific electrostatic guidance

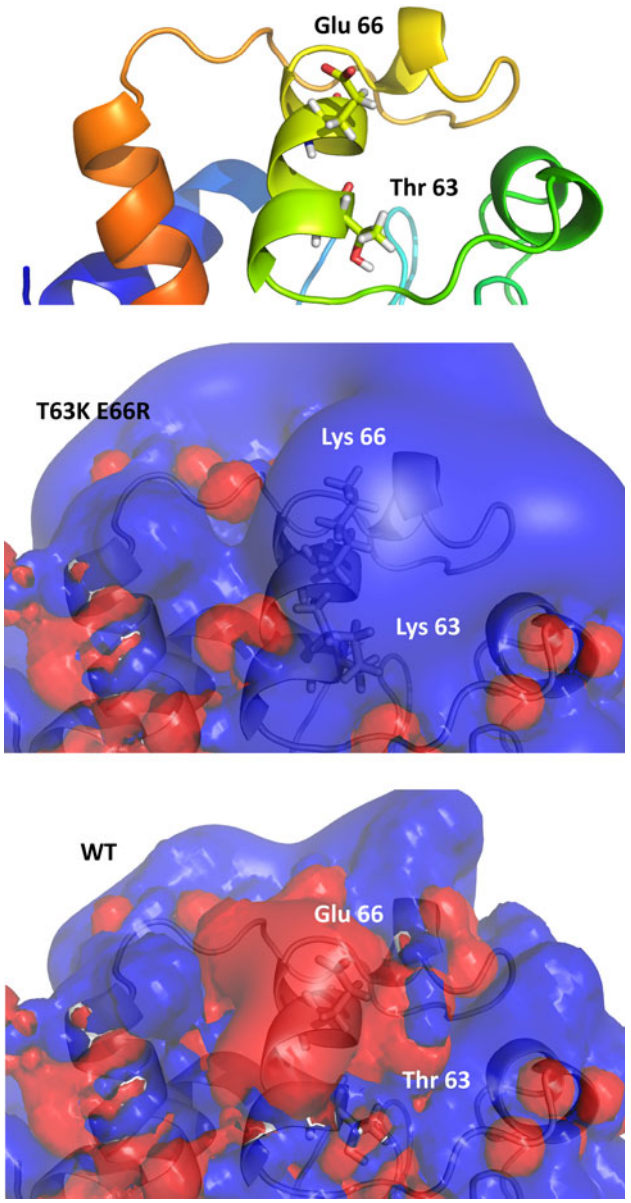

Fig. 5 Surface potential representation of the area around residues 63 and 66 in human cytochrome *c*: regions where the electrostatic potential is less than −1 *kT*/*e* are in *red*, whereas those where it is greater than 2 *kT*/*e* are in *blue*. The wild type and the T63K-E66K variant are represented in the *bottom panel* and the *middle panel*, respectively. The residues at positions 63 and 66 are shown as sticks and visible in transparency. Residue labels have been added at the terminal part of the side chain to show their orientation. In the *top panel* the same cartoon representation as in Fig. 1 is used to help localize the analyzed areas on the whole protein structure. As in Fig. 4, the backbone (cartoon) and side chains of mutated residues (sticks) are visible in transparency

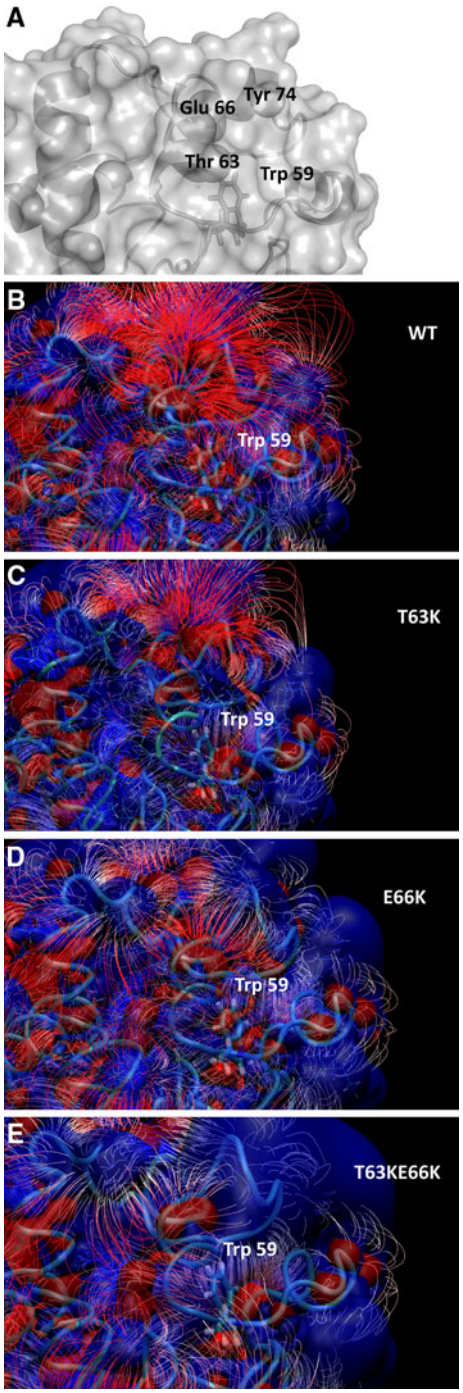

Fig. 6 The *top panel* represents the investigated protein surface area, where a cavity is identified having residues in the top part of its rim. The other panels represent surface potential and field lines in, from *top* to *bottom*, the wild-type protein, the T63K mutant, the E66K mutant, and the E66K-T63K mutant. Comparison of the electrostatic potential in human cytochrome *c* and some of its variants in the area around residues 63 and 66. Electrostatic potential isosurfaces less than −1 *kT*/*e* are in *red*, whereas those greater than 2 *kT*/*e* are in *blue*

toward an entry point located in a protein area that is known to be characterized by the largest internal mobility. The electrostatic attraction is determined by proper orientation of the introduced positively charged side chains.

Additionally, it is found that a structural opening can also increase the access of superoxide to the reaction center (e.g., F82K mutant). Although the reaction rate is

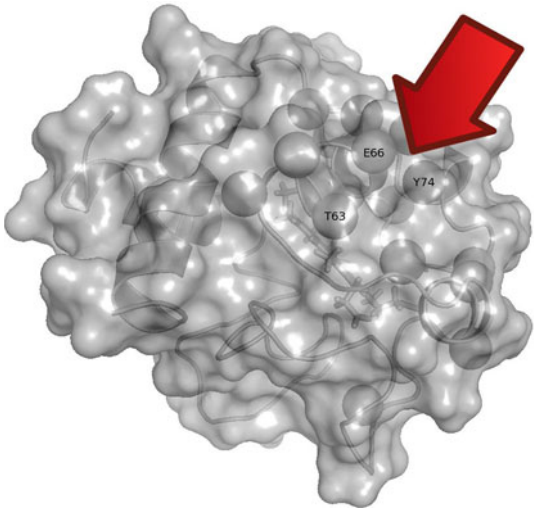

Fig. 7 The surface of cytochrome *c* presents a small cavity with a rim defined by residues T63, E66, and Y74. The cartoon representation of the protein structure with spheres for mutated residues reported in Fig. 1 is visible here in transparency

increased, other properties (e.g., surface coverage) may be altered.

For application in a sensor, the cytochrome *c* mutants have to be immobilized on modified gold electrodes allowing direct electron transfer between the electrode and the heme group. Here structural integrity is important to avoid altered redox properties and unfavorable orientation of the proteins. Only by fulfilling these preconditions can an enhanced reaction rate be used for improved detection for the superoxide anion radical.

Acknowledgments We thank the Bio-NMR project (European FP7 Collaborative Project and Coordination – Support Action, contract no. 261863) for access to the NMR instrumentation. The WeNMR project (European FP7 e-Infrastructure grant, contract no. 261572, http://www.wenmr.eu), supported by the national GRID Initiatives of Belgium, France, Italy, Germany, the Netherlands (via the Dutch BiG Grid project), Portugal, Spain, the UK, South Africa, Taiwan, and the Latin America GRID infrastructure via the Gisela project is acknowledged for the use of web portals and computing and storage facilities. The work was also partially supported by the German research association DFG (project LI 706/7-1).

References

1. Valko M, Leibfritz D, Moncol J, Cronin MTD, Mazur M, Telser J (2007) Internat J Biochem Cell Biol 39:44–84
2. Rosen GM, Britigan BE, Halpern HJ, Pou S (1999) Free radicals: biology and detection by spin trapping. Oxford University Press, New York
3. Balaban RS, Nemoto S, Finkel T (2005) Cell 120:483–495
4. Culotta VC, Yang M, O'Halloran TV (2006) Biochem Biophys Acta 1763:747–758
5. Faraci FM, Didion SP (2004) Arterioscler Thromb Vasc Biol 24:1367–1373
6. Valentine JS, Doucette PA, Potter SZ (2005) Annu Rev Biochem 74:563–593
7. Cave AC, Brewer AC, Narayanppanicker A, Ray R, Grieve DJ, Walker S, Shah AM (2006) Antioxid Redox Signal 8:691–728
8. Mariani E, Polidori MC, Cherubini A, Mecocci P (2005) J Chromatogr B 827:65–75
9. Venardos KM, Perkins A, Headrick K, Kaye DM (2007) Curr Med Chem 14:1539–1549
10. Slemmer JE, Shacka JJ, Sweeney MI, Weber JT (2008) Curr Med Chem 15:404–414
11. Li JM, Shah AM (2004) Am J Physiol Regul Integr Comp Physiol 287:1014–1030
12. Butler J, Jayson GG, Swallow AJ (1975) Biochim Biophys Acta 408:215–222
13. McCord JM, Fridovich I (1969) J Biol Chem 244:6049–6055
14. Jr Martin, Joseph P (1990) Methods Enzymol 186:220–227
15. Beissenhirtz MK, Scheller FW, Lisdat F (2004) Anal Chem 76:4665–4671
16. Gobi KV, Mizutani F (2000) J Electroanal Chem 484:172–181
17. Chang SC, Pereira-Rodrigues N, Henderson JR, Cole A, Bedioui F, McNeil CJ (2005) Biosens Bioelectron 21:917–922
18. Manning P, Cookson MR, Eggett CJ, Tolias CM, Read SJ, Hunter AJ, Tsatmail M, Thody AJ, Hillhouse EW, Shaw PJ, McNeil CJ (2000) Analusis 28:493–505
19. Büttemeyer R, Philipp AW, Schlenzka L, Mall JW, Beissenhirtz M, Lisdat F (2003) Transpl Proc 35:3116–3120
20. Ohsaka T, Tian Y, Shioda M, Kasahara S (2002) Chem Commun 990–991
21. Beissenhirtz MK, Sheller FW, Viezzoli MS, Lisdat F (2006) Anal Chem 78:928–935
22. Wegerich F, Turano P, Allegrozzi M, Möhwald H, Lisdat F (2009) Anal Chem 81:2976–2984
23. Banci L, Bertini I, Dikiy A, Kastrau DHW, Luchinat C, Sompornpisut P (1995) Biochemistry 34:206–219
24. Bren KL, Gray HB, Banci L, Bertini I, Turano P (1995) J Am Chem Soc 117:8067–8073
25. Banci L, Bertini I, Spyroulias GA, Turano P (1998) Eur J Inorg Chem 1998:583–591
26. Sakamoto K, Kamiya M, Uchida T, Kawano K, Ishimori K (2010) Biochem Biophys Res Commun 398:231–236
27. Barker PD, Bertini I, Del Conte R, Ferguson SJ, Hajieva P, Tomlinson EJ, Turano P, Viezzoli MS (2001) Eur J Biochem 268:4468–4476
28. Fetrow JS, Baxter SM (1999) Biochemistry 38:4480–4492
29. Baxter SM, Fetrow JS (1999) Biochemistry 38:4493–4503
30. Banci L, Gori Savellini G, Turano P (1997) Eur J Biochem 249:716–723
31. Bortolotti CA, Amadei A, Aschi M, Borsari M, Corni S, Sola M, Daidone I (2012) J Am Chem Soc 134:13670–13678
32. Bertini I, Chevance S, Del Conte R, Lalli D, Turano P (2011) Plos ONE 6:18329
33. Ge B, Lisdat F (2002) Anal Chim Acta 454:53–64
34. Behar D, Czapski G, Rabani J, Dorfman L, Schwarz H (1970) J Phys Chem 74:3209–3213
35. Bard AJ, Faulkner LR (2001) Electrochemical methods: fundamentals and applications, 2nd edn. John Wiley & Sons, New York
36. Laviron E (1979) J Electroanal Chem 101:19–28
37. Jeng WY, Chen CY, Chang HC, Chuang WJ (2002) J Bioenerg Biomembr 34:423–431
38. Case DA, Darden TA, Cheatham TE, Simmerling CL, Wang J, Duke RE, Luo R, Merz KM, Wang B, Pearlman DA, Crowley M, Brozell S, Tsui V, Gohlke H, Mongan J, Hornak V, Cui G, Beroza P, Schafmeister CE, Caldwell JW, Ross WS, Kollman PA (2008) AMBER 10. University of California, San Francisco

39. Hornak V, Abel R, Okur A, Strockbine B, Roitberg A, Simmerling C (2006) Proteins 65:712–725
40. Giachetti A, La Penna G, Perico A, Banci L (2004) Biophys J 87:498–512
41. Jayaram B, Sprous D, Beveridge DL (1998) J Phys Chem B 102:9571–9576
42. Bertini I, Case DA, Ferella L, Giachetti A, Rosato A (2011) Bioinformatics 27:2384–2390
43. Baker NA, Sept D, Joseph S, Holst MJ, Mc Cammon JA (2001) Proc Natl Acad Sci USA 98:10037–10041
44. Humphrey W, Dalke A, Schulten K (1996) J Mol Graph 14: 33–38
45. Xu J, Bowden EF (2006) J Am Chem Soc 128:6813–6822
46. Davis AV, O'Halloran TV (2008) Nat Chem Biol 4:148–151
47. Wegerich F, Turano P, Allegrozzi M, Möhwald H, Lisdat F (2011) Langmuir 27:4202–4211